Fast Fourier transform computational method for the propagation of electromagnetic pulses through layered dielectric media

Burke Ritchie and Michael D. Feit
Lawrence Livermore National Laboratory, University of California, Livermore, California 94550
(Received 9 February 1995; revised manuscript received 8 May 1995)

A computational method is developed for solving the wave equation for the propagation of a pulse through layered dielectric media. The method is based on an *ansatz* for evaluating fields in each layer after a temporal interval dt using a Fourier method. The resulting spatial fields represent the solution to the wave equation provided dt is small enough that many temporal intervals are required for the passage of the pulse through a boundary.

PACS number(s): 02.70.−c, 41.20.Jb

I. INTRODUCTION

Many problems in electromagnetic propagation involve passing a pulse through regions of uniform dielectric separated by sharp boundaries [1]. If the radiation could be described by plane waves, then such a problem would be analytically solvable. However, for pulses, numerical methods are used, and finite-difference methods that solve the coupled first-order, vector Maxwell equations, with explicit boundary matching, seem to be in wide use [1]. In this paper we propose and benchmark (albeit for the scalar and two-component wave equations) a method that takes full advantage of the nature of the problem, namely, regions of uniform dielectric separated by sharp boundaries. The method is based on an ansatz that Maxwell's equations in Fourier-transform space, comprising a set for each dielectric region, which are solved analytically in the time, can be propagated throughout the entire region, with satisfaction of the boundary conditions to high accuracy, simply by back-transforming each set exclusively into its own region of dielectric. This solution is accomplished over a series of temporal intervals dt, where high accuracy is obtained provided many intervals are used to pass the pulse through a boundary or series of boundaries. Thus the pulse width should be large compared to a distance vdt, where v is some average phase velocity appropriate for the dielectric media in the vicinity of the pulse. The pulse does not have to be large compared to a wavelength [i.e., the method is not a slowly varying envelope approximation in time (SVEAT) [2]], and the method preserves the phase velocity of the pulse in each region to high accuracy (the average velocity referred to above being simply a parameter used to define a characteristic distance over a temporal interval).

The equation one must solve subject to appropriate boundary conditions is

$$[\nabla^2\vec{E}-\vec{\nabla}(\vec{\nabla}\cdot\vec{E})-\frac{1}{c^2}\frac{\partial^2}{\partial t^2}(\varepsilon\vec{E})]=\vec{0}\ . \tag{1}$$

It is no problem to solve this equation exactly for the propagation of monochromatic fields, i.e., $(\partial^2/\partial t^2)(\varepsilon E)=-\varepsilon\omega^2 E$, and one can solve an equation like this one for each frequency ω and match the solutions appropriately at the boundaries. However, this method becomes inefficient for a broadband pulse. Our method is most appropriate therefore for pulses a few wavelengths long (wide bandwidth).

The presence of a function of space, namely, the dielectric function ε, in the term containing the time derivative puts the equation in a nonstandard form with respect to numerical algorithms developed in optical physics [2]. For example, the field can be expanded,

$$\vec{E}=\tfrac{1}{2}(\vec{\varepsilon}e^{-i\omega t}+\text{c.c.})\ , \tag{2a}$$

where ω is the carrier frequency of the incident field, and on substitution into Eq. (1) one makes the SVEAT [2] approximation by dropping the second-order time derivative of the envelope $\vec{\varepsilon}$, which is now assumed to be many wavelengths long, as small compared to ω times the first-order time derivative of the envelope. The dielectric function is written $\varepsilon=n^2=1+4\pi\chi$, where n is the index of refraction and χ is the linear susceptibility. The polarization is defined as $P=\chi E$. Then in the SVEAT development [2] one has the equation

$$\frac{\partial^2}{\partial t^2}P=\frac{\partial^2}{\partial t^2}(\chi\varepsilon e^{-i\omega t}+\text{c.c.})\ . \tag{2b}$$

In SVEAT [2] one can formally drop $\chi\omega$ times the first-order time derivative of the envelope as small compared to $\chi\omega^2$ times the envelope. This puts the equation in the standard parabolic or Schrödinger form [2]; however, the inherent error in this procedure is that the parabolic equation makes the pulse move at the same average velocity in all media. Different media correspond to different phase velocities. If only a small change in refractive index occurs in passing from one medium into another, then this is not a serious error in the usual SVEAT [2].

Nonlinear optical effects can be included in our formulation by operator splitting. That is, one alternates between small time steps of free propagation and nonlinear phase accumulation [3]. This approach is already common in situations such as harmonic generation or optical

parametric amplification, in which the total field cannot be described by a single slowly varying envelope.

Our method depends on our ability to Fourier transform Maxwell's equations in space at an initial time. Then we use these wave amplitudes to represent the field in each layer, although at initial time these layers are at some distance from an initial layer (air, for example) containing the initial pulse. We then solve these equations analytically in transform space for each dielectric layer over a time interval dt and backtransform into each region of separate dielectric to reconstruct the spatial field. This procedure is repeated for each dt interval—one forward transform over all space and j backtransforms into j separate dielectric layers. The resulting spatial field passes smoothly through the various boundaries and accurately represent a solution to Maxwell's equations if dt is small enough that the passage of a pulse through a boundary takes place over many dt intervals. In practice this means that $cdt/n_{\rm av} \ll w$, where $n_{\rm av}$ is the average of the different dielectric constants of two or more layers and w is the width of the incident pulse. If this condition is satisfied, then the boundary conditions of the problem are approximately satisfied, as we shall see. In other words the procedure avoids the explicit boundary matching required in a direct spatial solution [1]. In some sense the method also achieves the result of methods [2–4] in which the dielectric boundaries are replaced by a smooth function that varies rapidly over a wavelength since in this procedure also the interslab boundary conditions are not explicitly invoked. Later we present an error analysis that shows that the error of this procedure is of order dt^2, due to surface terms at a boundary during Fourier transformation, terms that we drop.

In summary, we present a propagation algorithm appropriate for the strongly refractive, the strongly reflective, and the vector nature of Eq. (1). The method is first presented for the scalar wave equation second order in space and time, a case that describes the propagation of TE modes in a slab, for which the second term in Eq. (1) is zero. Then we present a generalization to a case in which two vector components of Maxwell's equations are coupled, a case that describes the propagation of TM modes in a slab. These calculations are simple enough to demonstrate the computational method and are benchmarked against analytic results. Although the TM problem can be recast in the form of a scalar equation for the magnetic field, it is still a limited test case, for the electric field, to test our ability to solve the two-component form of the Maxwell vector equations and describe the situation in which the electric field is discontinuous across a boundary. However, we believe that the applicability of our computational method extends in principle to the full vector set. Finally, we also benchmark a calculation for two dielectric boundaries, i.e., three dielectric layers.

II. COMPUTATIONAL METHOD AND RESULTS

A. Propagation of TE modes

We illustrate our method by solving the wave equation for a slab in x and z (transverse and propagation directions, respectively) for an electric field polarized along y, E_y, and magnetic fields H_x and H_z. In region (1) with refractive index n_1 the equation for the electric field is

$$\left[\frac{\partial^2}{\partial x^2}+\frac{\partial^2}{\partial z^2}-\frac{n_1^2}{c^2}\frac{\partial^2}{\partial t^2}\right]E_y=0\ , \tag{3}$$

where the magnetic fields have been eliminated in favor of the single electric field. The spatial Fourier transform of Eq. (3) is

$$\left[\frac{n_1^2}{c^2}\frac{\partial^2}{\partial t^2}+k^2\right]\tilde{E}_y=0\ , \tag{4a}$$

$$k^2=k_x^2+k_z^2\ . \tag{4b}$$

At $t=0$, E_y is chosen to be a time-independent Gaussian centered on the forward-going plane wave, $e^{i(n_1k_0z-\omega t)}$, where $k_0=\omega/c$.

Consider a region of dielectric n_2 whose boundary is located at $z=0$ (Fig. 1) and thus is remote from the pulse at initial time. We write the equation in transform space,

$$\left[\frac{n_2^2}{c^2}\frac{\partial^2}{\partial t^2}+k^2\right]\tilde{F}_y=0\ . \tag{5}$$

The solutions of the two equations are written down analytically for forward propagation over an interval dt,

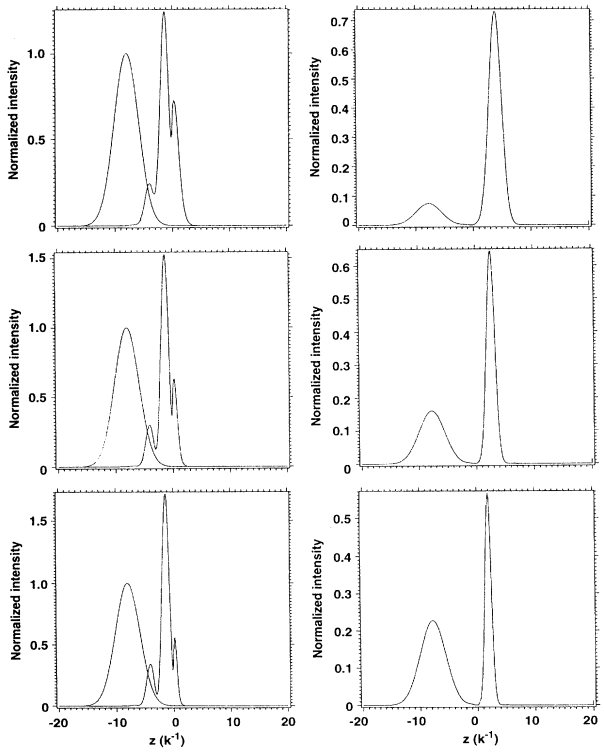

FIG. 1. Pulse intensity vs z at $t=0$ and $t_{\rm max}/2$ (left side) and at $t_{\rm max}$ (right side) for $n_1=1$ and $n_2=2$ (top), $n_2=3$ (middle), and $n_2=4$ (bottom). $t_{\rm max}=16$.

$$\tilde{E}_y = e^{-ikcdt/n_1}\tilde{E}_y^0 , \tag{6a}$$

$$\tilde{F}_y = e^{-ikcdt/n_2}\tilde{E}_y^0 , \tag{6b}$$

where $\tilde{E}_y^0$ is the transform from the previous step. The updated field is constructed by backtransforming $\tilde{E}_y$ and $\tilde{F}_y$ into the half spaces $z<0$ and $z>0$, respectively. The cycle is repeated for each dt. For the first step $\tilde{E}_y^0$ is just the transform of the initial pulse.

The error inherent in this procedure can be analyzed by considering the term at the boundary $z_0=0$ in Eq. (4a) or Eq. (5), which we have dropped as negligible. With reference to the former, where for simplicity we consider only the z dimension, zero on the right-hand side is replaced by

$$R = e^{-ikz_0}[(dE_y/dz)_{z_0} + ikE_y(z_0)] . \tag{7}$$

We assume that the field and its derivative at the boundary are known from a previous time step. Solving the inhomogeneous equation in transform space over an interval dt, the solution has the form of Eq. (6a) plus the remainder,

$$\tilde{E}_y' = \frac{R}{k^2}[1-\cos(kcdt/n_1)] , \tag{8}$$

where the term in brackets in Eq. (7) has been held constant over the interval dt. On expanding the cosine in Eq. (8) it is seen that this contribution is of order $R/2(cdt/n_1)^2$ and is neglected relative to $-i\tilde{E}_y^0 kcdt/n_1$ from the form of Eq. (6a).

Henceforth we use the scaled variables $x_s, z_s = k_0 x, k_0 z$ and $t_s = \omega t$ and drop the subscripts in subsequent discussions. In the numerical examples the widths of the initial Gaussian are taken as $4k^{-1}$ and $3k^{-1}$ in the x and z directions, respectively. This means that the full width at half maximum in the z direction in the plotted intensities below is $2\sigma\sqrt{\ln 2}$, where σ is the quoted Gaussian width (i.e., $3k^{-1}$ in Figs. 1 and 2 and $20k^{-1}$ in Figs. 7 and 8). In the calculations shown in Figs. 1 and 3 the numbers of spatial grid points are 257 and 513 for total grid sizes of $50k^{-1}$ and $40k^{-1}$ in the x and z directions, respectively, and the number of temporal grid points is 401 for $t_{\max} = 16\omega^{-1}$. In the calculation shown in Figs. 2 and 5, the total grid size in the z direction is $64k^{-1}$ and the number of grid points in this direction is 1025, everything else remaining the same as in Figs. 1 and 3. In Fig. 4, $t_{\max} = 32\omega^{-1}$ and the total grid size in the z direction is $128k^{-1}$, with no change in the number of grid points. We have used a version of the fast Fourier transform (FFT) code [5] in these calculations.

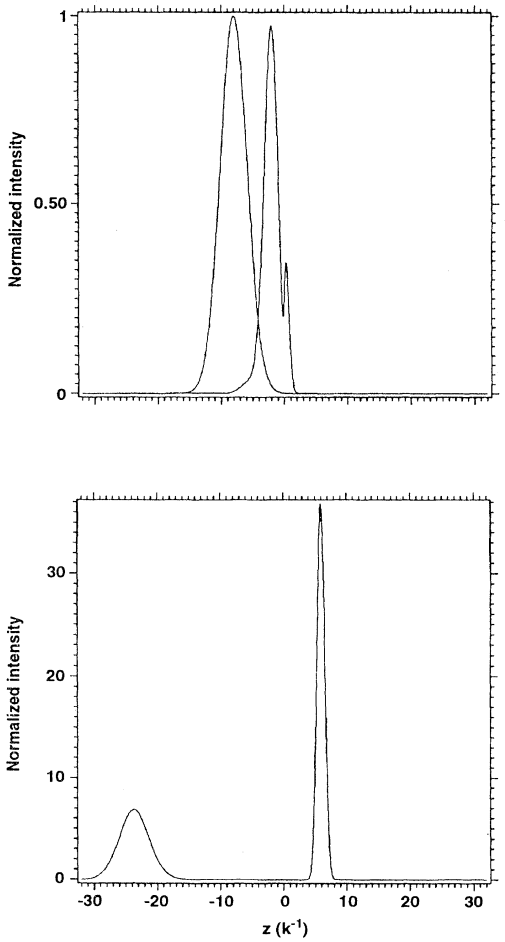

FIG. 2. Pulse intensity vs z at $t=0$ and $t_{\max}/4$ (top) and at $t_{\max}$ (bottom) for $n_1 = \frac{1}{2}$ and $n_2 = 2$. $t_{\max} = 16$.

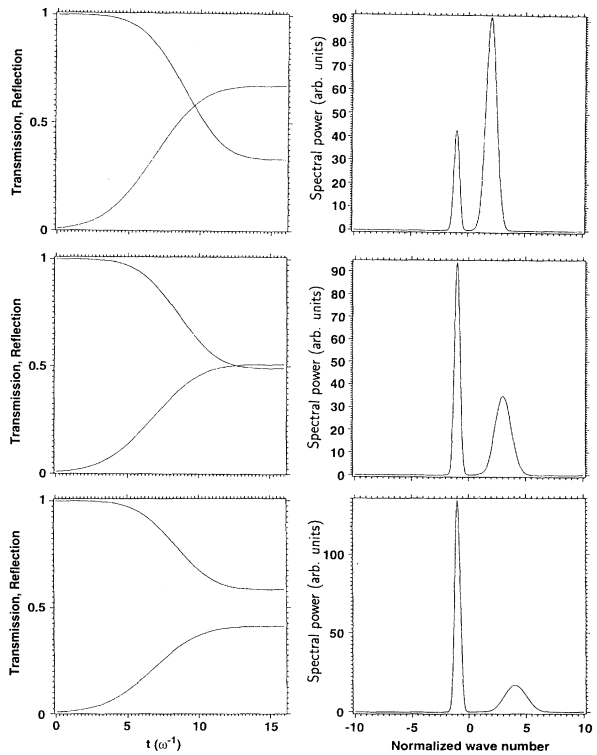

FIG. 3. Reflection (upper curve) and transmission (lower curve) coefficients for $n_1=1$ and $n_2=2$ (top left), $n_2=3$ (middle left), and $n_2=4$ (bottom left). Spectral power for $n_1=1$ and $n_2=2$ (top right), $n_2=3$ (middle right), and $n_2=4$ (bottom right).

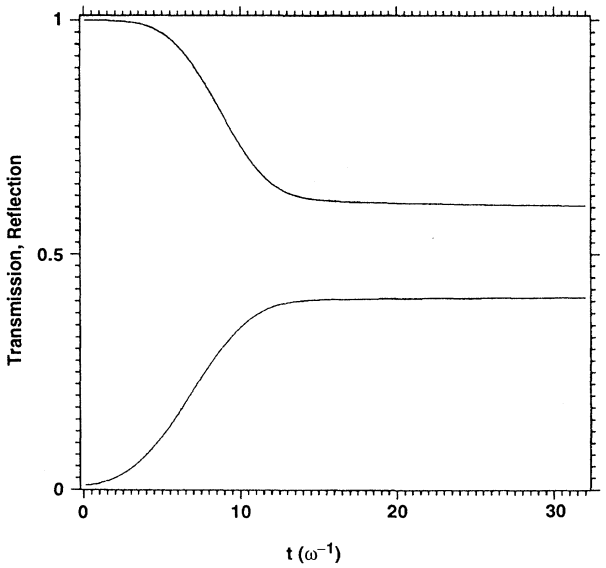

FIG. 4. Reflection (upper curve) and transmission (lower curve) coefficients for $n_1=\frac{1}{2}$ and $n_2=2$.

Our results are shown in Figs. 1–5. Figures 1 (left side) and 2 (top) show the initial pulse and the pulse athwart the boundary. In the latter snapshot, cleavage of the pulse at the boundary to produce the transmitted pulse is clearly visible and in Fig. 1 the emergence of the reflected pulse from the backside of the incident pulse is also visible. Figure 1 (right-hand side) and Fig. 2 (bottom) at maximum time show the reflected and transmitted pulses, where to very high accuracy the reflected pulse has traveled backward to the starting point at $-8k^{-1}$ appropriate for cleavage at $t_{\max}/2$ for $n_1=1$ (Fig. 1) and to $-24k^{-1}$ appropriate for cleavage at $t_{\max}/4$ (where $t_{\max}=16\omega^{-1}$) for $n_1=\frac{1}{2}$ (Fig. 2). Likewise the transmitted pulse has traveled forward for $t_{\max}/2$ divided by $n_2=2,3,4$ (Fig. 1) and $3t_{\max}/4$ divided by $n_2=2$ (Fig. 2).

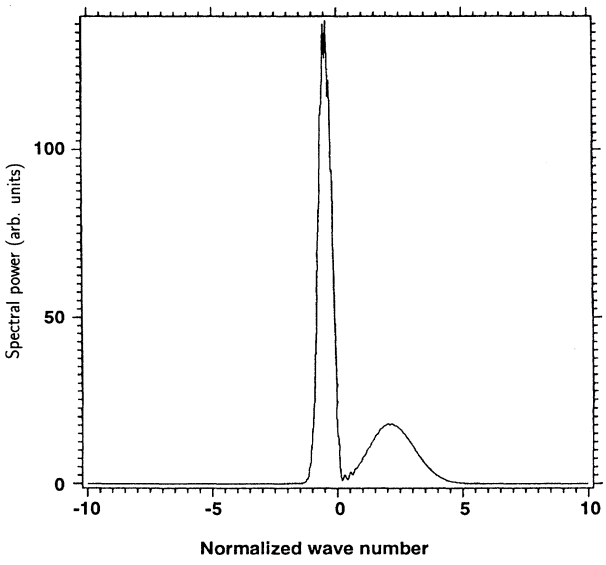

FIG. 5. Spectral power for $n_1=\frac{1}{2}$ and $n_2=2$.

The reflected and transmitted energies are measured from the integral over x and z of the squared modulus of the field. Figure 3 (left side) and Fig. 4 show the square root of the normalized energy in the region $x<0$ (top curve) and $x>0$ (bottom curve). At maximum time these agree to good accuracy with the formulas [6] $R=(n_2-n_1)/(n_2+n_1)$ and $T=2n_1/(n_2+n_1)$, respectively for plane waves with normal incidence on the boundary.

Figure 3 (right-hand side) and Fig. 5 show the spectral power, defined as the squared modulus of the axial Fourier transform of the field. The positions of the peaks give to very high accuracy normalized wave numbers, equal to the indices of refraction in the transmitted region on the right-hand side of the origin and equal to the negative of the indices of refraction in the reflected region to the left of the origin.

Finally the propagation method satisfies to high accuracy a conservation theorem that the time required for the pulse to traverse a given point is the same in both regions of dielectric. This causes the shape of the transmitted pulse to be compressed in the z direction (Figs. 1 and 2) such that its new width is n_1w_1/n_2, giving to high accuracy the conservation statement $z=ct/n_j$. This rule is observed to hold in all of the propagation snapshots, and correspondingly the spectra (Figs. 3 and 5) are observed to broaden. For example, the small oscillations near 0 in Fig. 5 reflect an interference in the spectrum of the reflected and transmitted waves for normalized wave numbers $-\frac{1}{2}$ and 2, respectively, where the overlap occurs because the spectral power of the transmitted wave is very broad, having the same width as the spectral power of the transmitted wave in the -1 and 4 case in Fig. 3. In other words the index jump is the same in both cases, 4, giving the same spectral width, but line center is at 2 in the former case such that the overlap of the reflected and transmitted parts of the spectrum occurs.

B. Propagation of TM modes

The propagation of TE modes in a slab involves only a single vector component of Maxwell's equations. A more stringent test of the generality of our computational method is the propagation of TM modes because then the electric vector is discontinuous across the boundary. For the same geometry as that in Sec. II A this calculation requires that we solve the pair of coupled equations for vector components E_x and E_z,

$$\left[\frac{\partial^2}{\partial z^2}-\frac{n_1^2}{c^2}\frac{\partial^2}{\partial t^2}\right]E_x=\frac{\partial^2 E_z}{\partial x\,\partial z}\ , \tag{9a}$$

$$\left[\frac{\partial^2}{\partial x^2}-\frac{n_1^2}{c^2}\frac{\partial^2}{\partial t^2}\right]E_z=\frac{\partial^2 E_x}{\partial z\,\partial x}\ . \tag{9b}$$

The Fourier transform of this pair can be diagonalized and solved analytically. In transform space the solutions can be expressed in terms of the TE solution that we obtained in Sec. II A,

$$\tilde{E}_x = \frac{k_z}{n_1}\tilde{E}_y \ , \tag{10a}$$

$$\tilde{E}_z = -\frac{k_x}{n_1}\tilde{E}_y \ . \tag{10b}$$

Equations (10a) and (10b) are solved in an interval dt and backtransformed into the appropriate spaces, as described in Sec. II A. For normal incidence on the boundary, as in Sec. II A, the result is the same because E_z does not exist. However, for non-normal incidence power is distributed between E_x and E_z. In our example we choose the initial plane wave in E_y to be $e^{i[n_1 k_0(z\cos\phi - x\sin\phi)-\omega t]}$, where $\phi = 45°$. Then the transmission and reflection coefficients are given by [6]

$$T = \frac{2n_1 n_2 \cos i}{n_2^2 \cos i + n_1\sqrt{n_2^2 - n_1^2\sin^2 i}} = 0.37 \quad \text{for} \quad i = 45° \ , \tag{11a}$$

$$R = \frac{n_2^2 \cos i - n_1\sqrt{n_2^2 - n_1^2\sin^2 i}}{n_2^2 \cos i + n_1\sqrt{n_2^2 - n_1^2\sin^2 i}} = 0.48 \quad \text{for} \quad i = 45° \ , \tag{11b}$$

where the values at 45° are for $n_1 = 1$ and $n_2 = 4$. For this calculation the numbers of spatial grid points are 257 and 257 for total grid sizes of $75k^{-1}$ and $60k^{-1}$ in the x and z directions, respectively, and the number of temporal grid points is 401 for $t_{\max} = 24\omega^{-1}$. The reflected and transmitted energies are measured from the integral over x and z of the squared modulus of the field E_x. (Note that the TE and TM propagations are identical to the plane-wave propagations with the E vector perpendicular and parallel to the plane of incidence, respectively, elucidated analytically by Jackson [6].) Figure 6 shows the square root of the normalized energy in the region $x > 0$ (bottom curve) and $x < 0$ (top curve). At maximum time these agree respectively to good accuracy with the formulas in Eqs. (11). Note that at initial time the normalization is less than 1 because energy is shared between E_x and E_z.

C. Propagation of TE modes through multiple boundaries

Yet another stringent test of the accuracy of our method is the propagation through more than one dielectric boundary, for which analytic results are readily available for plane waves and TE boundary conditions [7]. In cases A and B our Gaussian-pulse results were directly comparable to plane-wave results, which is obvious from the independence of the reflection-transmission formulas for plane waves on wave-number absolute value. This is not the case for the calculations shown in Figs. 7 and 8 in which a pulse propagates from a region of index 1 through region of index 2, which is $7.03k^{-1}$ units wide and then back into a region of index 1. First the transverse width of the pulse must be many wavelengths ($25k^{-1}$ here) so that the plane-wave results can be simulated by propagating the pulse through the dielectric layers over a distance much less than a Rayleigh range, which is $z_R = kw^2$ here, where $w = 25k^{-1}$. Also the length of the pulse ($20k^{-1}$ here) must be large compared to the width of the "potential well" through which the pulse is passed. Otherwise it will be distorted by multiple reflections or feedback, a transient phenomenon clearly not described in the cw limit appropriate for a plane-wave benchmark. Finally a quantitative comparison requires that the analytic formulas be averaged with respect to the distribution of wave numbers contained in the longitudinal Gaussian pulse. The appropriate average is achieved by integrating the product, (reflection amplitude

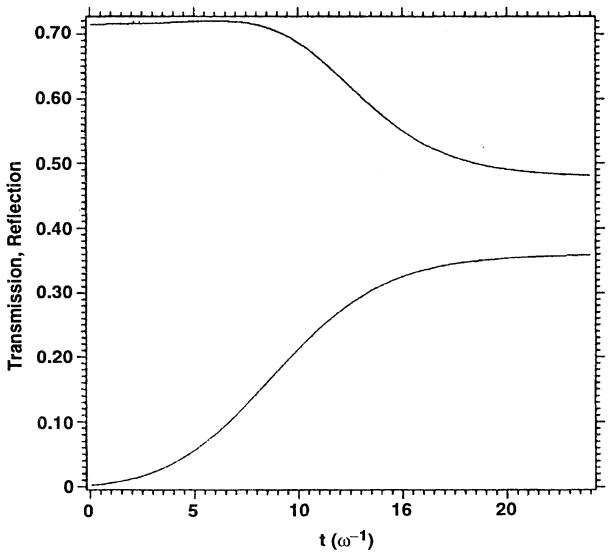

FIG. 6. Reflection (upper curve) and transmission (lower curve) coefficients for $n_1 = 1$ and $n_2 = 4$ for propagation of TM modes at non-normal incident angle of 45°.

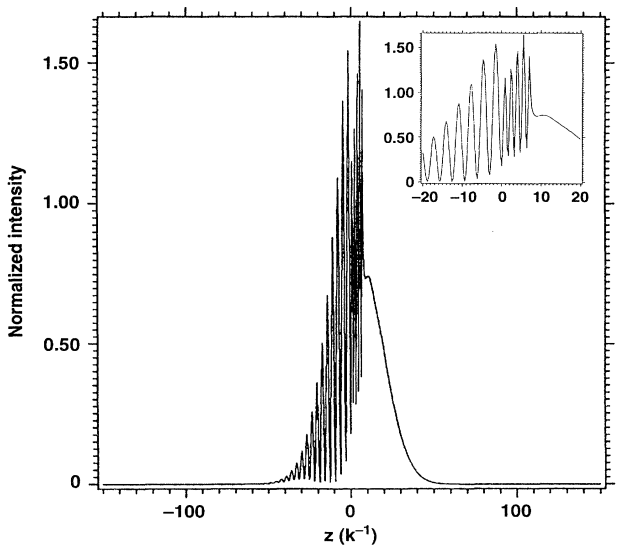

FIG. 7. Pulse intensity across a layer of higher index starting at 0 and ending at $7.03k^{-1}$. The inset shows a blowup near the layer.

× longitudinal Fourier transform of input field) over the momentum-space variable. In contrast, Patriarca [8] has shown how to inject a plane wave at a single spatial grid point such that his numerical result is compared with the analytic result at a single wave number.

Figure 7 shows an on-axis snapshot of the pulse being transmitted through and reflected from the dielectric layer starting at $z=0$ and ending at $z=7.03k^{-1}$. The inset gives a blowup of the interference fringes to the left of and within the layer. Since the squared modulus of the field is being plotted, twice the number of wavelengths appear. The wavelength within the layer is one-half the wavelength to the left of the boundary because of the 2:1 index ratio, respectively.

Figure 8 shows an on-axis snapshot of the reflected and transmitted pulses after separation. Conservation of energy is demonstrated by the sum of the peak heights to 1 to a good approximation. Also, the reflected peak height agrees well with the averaged plane-wave result of 0.231. Finally, conservation of energy is demonstrated again by the greater width of the reflected pulse, which is controlled by the group velocities in and out of the layer and is observed to be the sum of the incident pulsewidth and one-half the incident pulsewidth inside the layer caused by twice the index inside the layer.

In the calculations shown in Figs. 7 and 8 the number of temporal, transverse spatial, and longitudinal spatial grid points is 801, 257, and 1025 for maximum variable lengths of $175\omega^{-1}$, $150k^{-1}$, and $300k^{-1}$, respectively. It is found that the two-boundary calculation is an extremely sensitive test of the accuracy of the method.

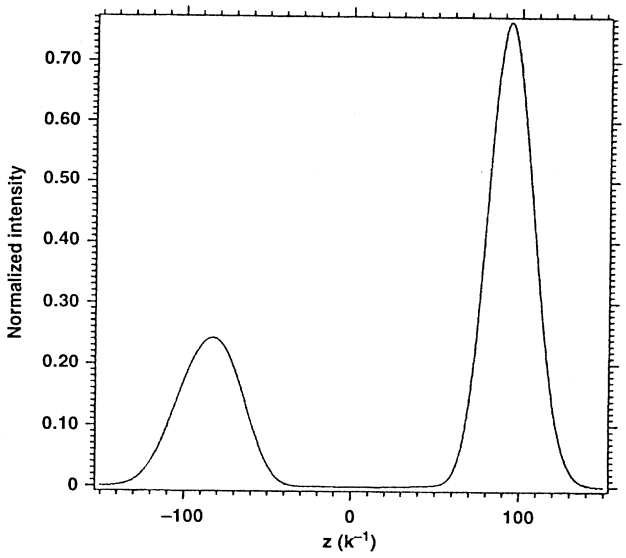

FIG. 8. Pulse intensity for propagation through a layer of higher index after separation of the reflected and transmitted pulses.

III. SUMMARY AND CONCLUSIONS

In this paper a computational method has been presented for solving Maxwell's equations in a space containing layered dielectrics. The method is based on temporally evolving the solutions in momentum space over an interval dt and then backtransforming into the regions of separate dielectric. It is demonstrated that the boundary conditions, although quite intricate for the vector set of equations, are approximately satisfied if cdt/n_{av} is small compared to the width of the incident pulse.

In Cartesian coordinates the method makes use of the standard FFT routine [5], which is very fast on a vector machine. The method is intended to replace finite-difference algorithms [1], which are prone to numerical instabilities and seem naturally unsuited to problems in which regions of constant dielectric are separated by sharp boundaries. The method is most useful for broad bandwidth pulses and in regions of strong refraction in which the change of index is large in passing through a boundary such that one cannot avoid the nonstandard (i.e., the nonparabolic) mathematical form in which a function of space multiplies the second- or first-order time derivative of the field.

ACKNOWLEDGMENTS

This work was performed under the auspices of the U.S. Department of Energy by Lawrence Livermore National Laboratory under Contract No. W-7405-ENG-48.

[1] Karl S. Kunz and Raymond J. Luebbers, *The Finite Difference Time Domain Method for Electromagnetics* (CRC Press, Boca Raton, 1993).

[2] M. Scalora and M. Crenshaw, Opt. Commun. **108**, 191 (1994).

[3] M. D. Feit and J. A. Fleck, Jr., J. Opt. Soc. Am. B **7**, 2048 (1990).

[4] J. A. Fleck, Jr., J. R. Morris, and M. D. Feit, Appl. Phys. **10**, 129 (1976); M. D. Feit and J. A. Fleck, Jr., Appl. Opt. **17**, 3990 (1978).

[5] J. W. Cooley and J. W. Tukuy, Math. Comp. **19**, 297 (1965).

[6] J. D. Jackson, *Classical Electrodynamics*, 2nd ed. (Wiley, New York, 1975), pp. 278–282.

[7] E. Merzbacher, *Quantum Mechanics* (Wiley, New York, 1961), pp. 105–106.

[8] M. Patriarca, Phys. Rev. E **50**, 1616 (1994).